

# Mice Lacking the Orphan Receptor Ror1 Have Distinct Skeletal Abnormalities and Are Growth Retarded

Natalia Lyashenko,<sup>1</sup> Martina Weissenböck,<sup>1</sup> Amnon Sharir,<sup>2</sup> Reinhold G. Erben,<sup>3</sup> Yasuhiro Minami,<sup>4</sup> and Christine Hartmann<sup>1\*</sup>

**Ror1 is a member of the Ror-family receptor tyrosine kinases. Ror1 is broadly expressed in various tissues and organs during mouse embryonic development. However, so far little is known about its function. The closely related family member Ror2 was shown to play a crucial role in skeletogenesis and has been shown to act as a co-receptor for Wnt5a mediating non-canonical Wnt-signaling. Previously, it has been shown that during embryonic development Ror1 acts in part redundantly with Ror2 in the skeletal and cardiovascular systems. In this study, we report that loss of the orphan receptor Ror1 results in a variety of phenotypic defects within the skeletal and urogenital systems and that *Ror1* mutant mice display a postnatal growth retardation phenotype. *Developmental Dynamics* 239:2266–2277, 2010. © 2010 Wiley-Liss, Inc.**

**Key words:** Ror1; postnatal growth retardation phenotype; skeletal defects; mice

Accepted 8 June 2010

## INTRODUCTION

Ror1 is one of the two vertebrate Ror-family members of orphan receptor-tyrosine kinases (Yoda et al., 2003; Green et al., 2008; Minami et al., 2009). Like its closely related family member Ror2, Ror1 contains an extracellular cysteine-rich domain (CRD) similar to the CRD domain of the Wnt-receptor frizzled (Saldanha et al., 1998). It has been demonstrated that Ror2 can bind to Wnt-ligands as well as to the BMP/TGFβ-family member, Gdf5 (Oishi et al., 2003; Sammar et al., 2004; Liu et al., 2008). Ror2 activity can mediate non-

canonical Wnt-signaling through interaction with Wnt5a, and modulates the canonical Wnt-signaling pathway through differential interaction with the Frizzled receptor (Hikasa et al., 2002; Mikels and Nusse, 2006; He et al., 2008; Li et al., 2008). Ror1 has been recently demonstrated to be capable of binding the Wnt5a ligand as well. However, whether this binding results in functional activity is currently not known (Fukuda et al., 2008). Both *Ror* genes are widely expressed during embryonic development, in limbs, perichondrium of the developing long bones,

teeth, heart, lung, liver, gut, urogenital tract, and hippocampal neurons (Oishi et al., 1999; Al-Shawi et al., 2001; Matsuda et al., 2001; Paganoni and Ferreira, 2003; Rodriguez-Niedenfuhr et al., 2004; Schwabe et al., 2004). Mutations in *ROR2* in humans cause autosomal dominant brachydactyly type B (BDB) and are associated with an autosomal recessive form of Robinow syndrome (RS) (Afzal et al., 2000; Oldridge et al., 2000; Schwabe et al., 2000; van Bokhoven et al., 2000; Hamamy et al., 2006). Loss of *Ror2* in mice results in phenotypic changes resembling RS (DeChiara et al., 2000;

Additional Supporting Information may be found in the online version of this article.

<sup>1</sup>Institute of Molecular Pathology, Vienna, Austria

<sup>2</sup>Department of Molecular Genetics, Weizmann Institute of Science, Rehovot, Israel

<sup>3</sup>Department of Biomedical Sciences, University of Veterinary Medicine, Vienna, Austria

<sup>4</sup>Division of Cell Physiology, Department of Physiology and Cell Biology, Graduate School of Medicine, Kobe University, Kobe, Japan

Grant sponsor: Boehringer Ingelheim; Grant sponsor: Austrian Science Fund; Grant number: P19281-B16; Grant sponsor: EU Network of Excellence: Cells into Organs; Grant number: LSHM-CT-2003-504468.

\*Correspondence to: Christine Hartmann, Institute of Molecular Pathology, Dr. Bohrgasse 7, 1030 Vienna, Austria.

E-mail: hartmann@imp.ac.at

DOI 10.1002/dvdy.22362

Published online 30 June 2010 in Wiley InterScience (www.interscience.wiley.com).

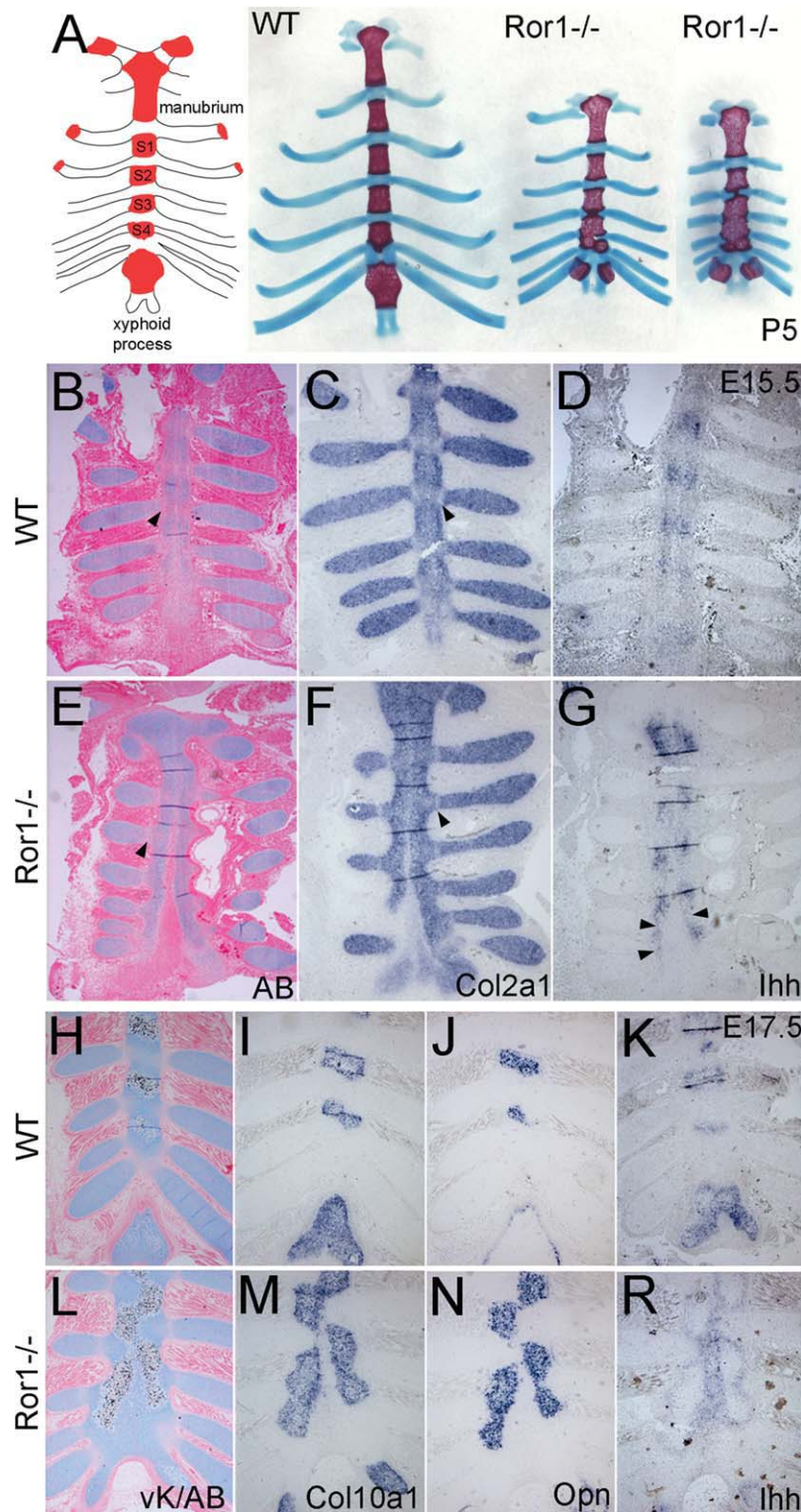


**Fig. 1.** Sternum defects in *Ror1* mutant mice. **A:** Schematic representation of the ossification centers in the sternum (colored in red), from rostral to caudal: manubrium, sternbrae (s) 1–4, xyphoid process. Alcian blue/alizarin red stained sterni with ribs of postnatal day 5 (P5) old wild-type (WT) and two *Ror1* mutant animals. **B–G:** Sections from E15.5 old wild-type (B–E) and mutant embryos (E–G), stained with alcian blue and eosin (B, E), hybridized with probes for *Col2a1* (C, F) and *Ihh* (D, G). Arrowheads in B, C, E, F indicate the normal (B, C) and abnormal (E, F) shape and location of the sternal-costal junctions. Arrowheads in G indicate the fused *Ihh* expression domain across two intercostals segments. **H–R:** Sections from E17.5 old wild-type (H–K) and mutant (L–R) embryos, stained with von Kossa / alcian blue (vK/AB) (H, L), or hybridized with probes for *Col10a1* (I, M), *Osteopontin* (*Opn*) (J, N) and *Ihh* (K, R).

Takeuchi et al., 2000; Schwabe et al., 2004). The point mutation *Ror2*-W749X, linked to human BDB, behaves as a recessive mutation in mouse causing brachydactyly and models recessive RS (Raz et al., 2008). In addition, ROR family member have been implicated in tumor formation in humans. ROR1 has been found to be overexpressed in patients with acute and chronic lymphoblastic leukemia (Shabani et al., 2007, 2008; Daneshmanesh et al., 2008) and was found to act as a survival kinase in HeLa cervical carcinoma cells (MacKeigan et al., 2005). ROR2 has been found to be overexpressed in squamous cell carcinoma, renal cell carcinoma, and metastatic melanoma, and to regulate osteosarcoma cell invasiveness (Enomoto et al., 2009; Kobayashi et al., 2009; Morioka et al., 2009; Wright et al., 2009; O'Connell et al., 2010). Previously it was reported that loss of *Ror1* in mice results in perinatal lethality due to respiratory defects, but that these mice lack any abnormalities in skeletogenesis (Nomi et al., 2001). Here, we have re-examined the *Ror1* mutants and found that the mice have subtle skeletal defects at birth; they showed fusions of the sternbrae, a cleft in the basisphenoid bone, and abnormal development of the cervical vertebral element C2. Homozygous mice survived in our facility and displayed abnormal synchondrosis in the cranial base, postnatal growth retardation, and age-related skeletal changes. Furthermore, we observed additional phenotypic defects in *Ror1*<sup>-/-</sup> mutants, such as female infertility probably due to an imperforated hymen, kidney defects, and occasionally enlarged seminal vesicles in *Ror1*<sup>-/-</sup> males.

## RESULTS

### Skeletal Defects in *Ror1*<sup>-/-</sup> Embryos

*Ror1* mutant embryos displayed very distinct skeletal defects, which were apparent prior to birth. The sternum of *Ror1*<sup>-/-</sup> embryos was shortened and showed fusion of caudal sternbrae (S) involving to a variable degree S1–S4 (Fig. 1A and Table 1). In addition, the xyphoid process was

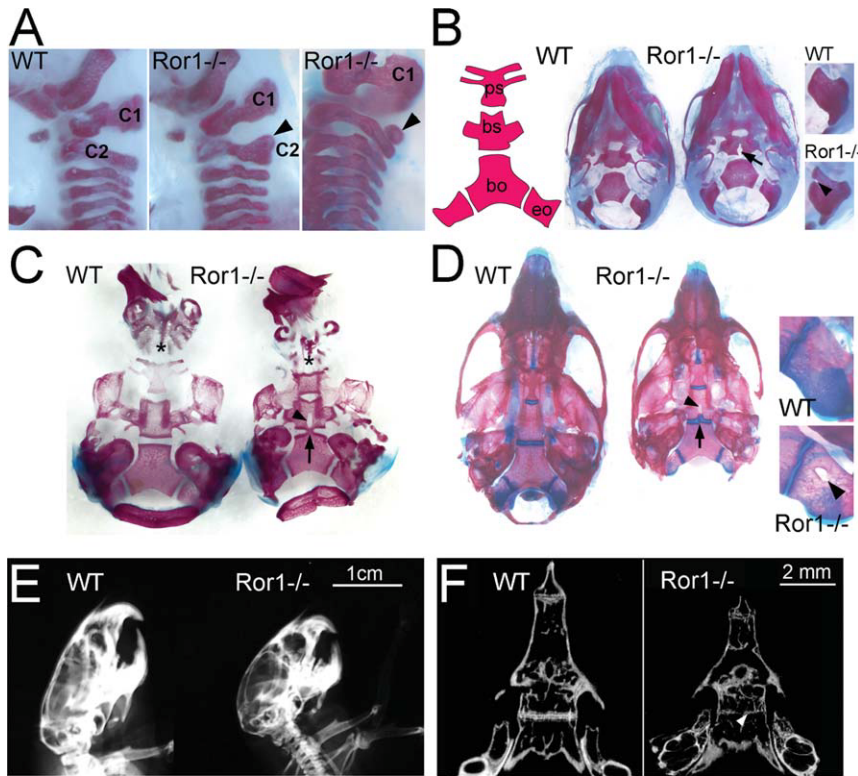


Fig. 2.

abnormally bifurcated showing two ossification centers in all mutants examined at birth or early postnatal stages (Fig. 1A). Defects in sternal development were already detectable at E15.5 where the two sternal bands were still separated from each other in the caudal region of *Ror1*<sup>-/-</sup> embryos, while they were already almost completely fused along the entire length in the wild-type littermate controls (Fig. 1B, E). The sternal-costal junctions, demarcations between the end of the ribs and the sternal tissue, can be distinguished by their reduced reactivity with the proteoglycan staining reagent alcian blue and low levels of *Collagen 2α1* (*Col2α1*) transcript, appeared right at the sternal bands in the wild-type (see arrowheads in Fig. 1C), while they were located more laterally in the *Ror1* mutants (Fig. 1F). In situ hybridization for the prehypertrophic marker, *Ihh*, revealed that the onset of chondrocyte differentiation occurs normally in the *Ror1* mutant sterni (Fig. 1D, G). However, in the caudal

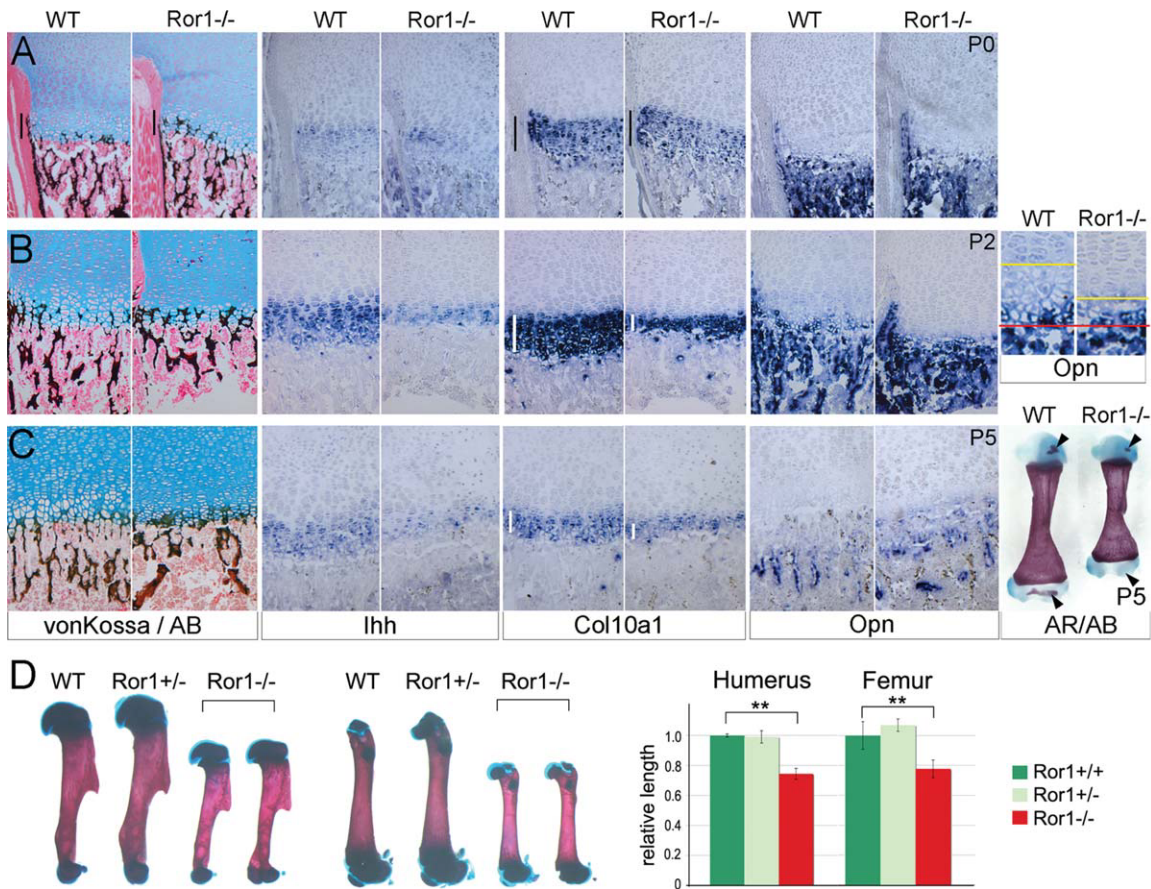


Fig. 3.

**TABLE 1. Summary of the Observed Sternebrae Fusion Defects in Mutant and Control (Wt/Het) Animals**

Genotype	s4+s3	s4-s2	s4-s1	s4-manubrium
Wt/Het (n=108) <sup>a</sup>	0	0	0	0
Mut (n=35)	12	14	8	1

<sup>a</sup>Occasionally a slight misalignment of sternum halves was observed (n=3; e.g. WT in Fig. 1C).

part the *Ihh* expression domains were not absolutely restricted to the intercostal segments (arrowheads in Fig. 1G). At E17.5, the abnormal shape and location of the sternal-costal junctions were still present in the mutant sterni. The sternal bands had either begun to fuse abnormally, visible by the presence of alcian blue–positive and *Col2α1* (not shown) –expressing cells in the midline, or were still separated by a small band of none-chondrogenic cells (data not shown). However, as in the wild-type, chondrocytes within the sternal bands had matured into hypertrophic chondrocytes that expressed *Collagen 10α1* (*Col10α1*) and *Osteopontin* (*Opn*) and produced mineralized matrix in all mutants examined (Fig. 1I, J, M, N). In contrast to the controls where this process was restricted to the intercostals regions, hypertrophic cells differentiated also

at the ends of ribs in the mutants leading to the formation of continuous hypertrophic domains in the region of sternebrae 3–4 (Fig. 1M, N). Concomitantly, *Ihh* expression was altered and expressed all around the hypertrophic regions (Fig. 1K, R). The abnormal expression of maturation markers, such as *Ihh* and *Col10α1*, suggests that the absence of functional *Ror1* affects the normal organization of cells into a growth plate-like structure in the intercostal regions of the sternum, instead those are now located at the costal-sternal junctions. This defect was even more apparent at P0 where *Col10α1* and *Ihh* were expressed almost all around the fused sternebrae elements, including the regions at the ends of the ribs (data not shown).

In addition to the defects in the sternum, we detected skeletal abnormalities in the cervical vertebral ele-

ment C2 and the base of the skull in newborns (P0). The cervical element C2 appeared wider in the mutants (n=9) and was split in some mutants (n=4/9; Fig. 2A). In the skulls of mutant newborns, clefts were present in the posterior region of the basisphenoid bone and in the anterior borders of the exoccipitale bones in 100% of the mutants analyzed (n=9; Fig. 2B). No alterations were found in the suture regions in the dorsum of the skull (data not shown). At P5, the clefts had developed into holes, which were still visible at later stages and in adults (Fig. 2C, D, and data not shown). Furthermore, we noticed in the cranium of P5 and P19 heads a bony bridge within the spheno-occipitale synchondrosis connecting the basioccipitale with the basisphenoid bone (arrows in Fig. 2C, D). This resulted in premature synostosis of the spheno-occipitale synchondrosis in the cranial base and an overall shortening of the skull with a more dome-shaped appearance in X-rays at the adult stage (Fig. 2E). At P5, it was also apparent that the vomeral bones were hypoplastic (Fig. 2C). In the P17 and P19 mutant heads, we noticed a hole in the exoccipitale bones, which probably was the result of the cleft already visible in the newborn skulls (n=5; Fig. 2D). The fusion of the

**Fig. 2.** Skull and vertebral defects in *Ror1* mutant mice. **A:** Cervical region of the axial skeleton of wild-type (WT) and two different *Ror1*<sup>-/-</sup> newborns (M1 and M2), with M1 showing a widening of the C2 element and M2 showing a split C2 element with a dorsal floating piece (arrowheads). **B:** Schematic view of the basal cranial bones (bo, basioccipitale; bs, basisphenoid; ps, presphenoid; eo, exoccipitale) and ventral view on alcian blue/alizarin red–stained skulls of wild-type and *Ror1*<sup>-/-</sup> newborns (P0), showing the cleft in the basisphenoid bone (arrow). The magnified regions on the right show the exoccipitale bone of wild-type (WT) and *Ror1*<sup>-/-</sup> (M), with the arrowhead pointing at the cleft in the mutant. **C:** Dorsal view on the alcian blue/alizarin red–stained base of a wild-type and mutant P5 old skull, after removal of the ventral flat bones. The arrow indicates the bony bridge between the basioccipitale and basisphenoid bone, the arrowhead points at the hole in the basisphenoid bone, and the asterisks mark the vomeral bones. Note: The alcian blue staining in this sample is almost not visible. **D:** Ventral view on alcian blue/alizarin red–stained skulls of wild-type and *Ror1*<sup>-/-</sup> P19 old mice, with the arrow pointing at the bony bridge between the basioccipitale and basisphenoid bone. The magnified regions on the right show the exoccipitale bone of wild-type (WT) and *Ror1*<sup>-/-</sup> (M), with the arrowhead pointing at the hole in the mutant. **E:** X-ray of 3-month-old mice showing the round, dome-like shape of the mutant skull in comparison to the wild-type. **F:** MicroCT image of the cranial base of wild-type and mutant 18-month-old animals, with the white arrowhead pointing at the synostosis of the basioccipitale and basisphenoid bones in the mutant.

**Fig. 3.** Postnatal growth plate phenotypes of *Ror1* mutants showing the proximal end of the humerus of wild type and *Ror1*<sup>-/-</sup> at P0, P2, and P5. **A:** P0 growth plate stained with von Kossa/alcian blue (AB) and hybridized with probes for *Ihh*, *Col10α1*, and *Opn*. Note there is no difference between wild type and mutant at this stage. Black bars indicate the zone of hypertrophic chondrocytes in the von Kossa/alcian blue staining and the *Col10α1* positive zone. **B:** P2 growth plate stained with von Kossa/alcian blue (AB) and hybridized with probes for *Ihh*, *Col10α1*, and *Opn*. Note the reduced size of the *Ihh*- and *Col10α1*-positive zones in the mutant compared to the wild type. White bars indicate the zone of *Col10α1*-positive hypertrophic chondrocytes. At the right, magnified regions of the P2 growth plates from WT and *Ror1*<sup>-/-</sup> hybridized with *Opn*, showing *Opn* expression throughout the zone of hypertrophic chondrocytes in the *Ror1* mutant. Yellow line indicates the border between the prehypertrophic/hypertrophic cells and the border between hypertrophic cells and the osteogenic front is indicated by the red line. **C:** P5 growth plate stained with von Kossa/alcian blue (AB) and hybridized with probes for *Ihh*, *Col10α1*, and *Opn*, showing reduced zones of *Ihh*- and *Col10α1*-positive cells in the mutant. White bars indicate the zone of *Col10α1*-positive hypertrophic chondrocytes. Alizarin red (AR)/alcian blue (AB)–stained wild-type and mutant humeri at P5, showing reduced or absent secondary ossification centers in the mutant (arrowheads). **D:** Alizarin red/alcian blue–stained wild-type, *Ror1* heterozygous, and *Ror1* mutant humeri and femora of littermates at P19 and bar graph showing the length difference based on the size measurements from three different litters (*Ror1*<sup>+/+</sup> n = 4; *Ror1*<sup>+/-</sup> n = 5; *Ror1*<sup>-/-</sup> n = 5). \*\**P* ≤ 0.003 (based on two-tailed Student's *t*-test).

basisphenoid and basioccipitale bone was also clearly visible by microCTs of aged mutant specimens (Fig. 2F). None of these skeletal defects was visible in heterozygous *Ror1* animals.

As previously described, *Ror1* is expressed at E10.5 and E11.5 in the developing limbs, somites, and head (see Supp. Fig. S1A,B, which is available online). At E12.5, we noticed a prominent expression of *Ror1* in the mesoderm of the body wall and at E13.5 in the sternal bars (see Supp. Fig. S1C–E). *Ror1* appears also to be expressed in perichondrium of the skeletal elements in the developing limb (see Supp. Fig. S1F, G). Furthermore, we noticed *Ror1* expression in the roof of the oral cavity and in the area of the developing pituitary gland (see Supp. Fig. S1H, I). Thus, *Ror1* is expressed in or near the skeletal elements/structures affected by the loss of *Ror1* activity.

Growth retardation of the *Ror1* mutant pups became apparent at P2 (see Fig. 4), associated with morphological and molecular changes in the growth plates of long bones (Fig. 3B), while there were no changes detectable at E17.5 or in newborns (Fig. 3A and data not shown). At P2, the prehypertrophic, *Ihh*-expressing, and the hypertrophic, *Col10 $\alpha$ 1*-expressing zones of the mutant growth plates were shorter compared to wild-type or heterozygous littermate controls (Fig. 3B). In the wild-type growth plates at P2, only the last 3–4 rows of hypertrophic chondrocytes had mineralized matrix, while the hypertrophic chondrocytes towards the articular region were slightly smaller and had a non-mineralized matrix (Fig. 3B). Similarly, *Opn* was expressed in the last 3–4 rows of hypertrophic chondrocytes in the wild-type growth plate (Fig. 3B). In contrast, in the *Ror1* mutant growth plate, only 3–4 rows of hypertrophic cells were present, which all expressed *Opn* and had a slightly hyper-mineralized matrix (Fig. 3B). Thus, loss of *Ror1* seems to affect the differentiation of a distinct subpopulation of hypertrophic cells and prehypertrophic chondrocytes. Examination of P5 specimens revealed a similar phenotype in the growth plate, with a hyper-mineralized matrix and reduced zones of *Ihh*- and *Col10 $\alpha$ 1*-expressing chondrocytes in the mutant (Fig. 3C). In addition, skeletal prepara-

tions as well as sections through the long bones revealed that the formation of the secondary ossification center was delayed in *Ror1* mutants (Fig. 3C and data not shown).

### **Ror1 Mutants Show Postnatal Growth Retardation and Have a Reduced Life Expectancy**

At postnatal day 2, *Ror1* mutant pups could easily be identified by their reduction in size and weight (Fig. 4A, B). Statistically significant reduction in the weight was apparent already at P1. However, the size reduction was less apparent at that age (Fig. 4A and data not shown). In contrast, no significant differences were detected between *Ror1* heterozygous and wild-type animals. Within the first 6 postnatal days, mutant pups reached only approximately 50% of the weight of their heterozygous and wild-type littermates (Fig. 4A). The life expectancy of the mutants was reduced; only 60% of the mutants (32/53) survived until weaning (Fig. 4C). The reduced life expectancy might in part be due to the occasional kidney defects (see below) or physical weakness of the runt pups compared to their littermates. *Ror1*<sup>-/-</sup> pups, which survived until after weaning, stayed smaller and reached only 60–75% of the weight of their littermates (Fig. 4D, E). Accordingly, their long bones were ~20% shorter compared to wild-type and heterozygous littermates (see Fig. 3D). X-rays of 3-month-old female mice suggested a decrease in bone density and in cortical thickness (Fig. 4D, see also inset). This finding prompted us to examine volumetric bone mineral density (BMD) and bone geometry by peripheral quantitative computed tomography. Femurs from *Ror1* mutant male and female mice were characterized by bonedensitometry, which revealed reductions in the cross-sectional area, total BMD, and cortical thickness in the shaft and metaphyseal region (Table 2). Cortical bone osteopenia at the femoral shaft might be slightly more pronounced in females than in males (Table 2). Likewise, the reduction in weight and size was more prominent in females than in males at the age of 3 months (Fig.

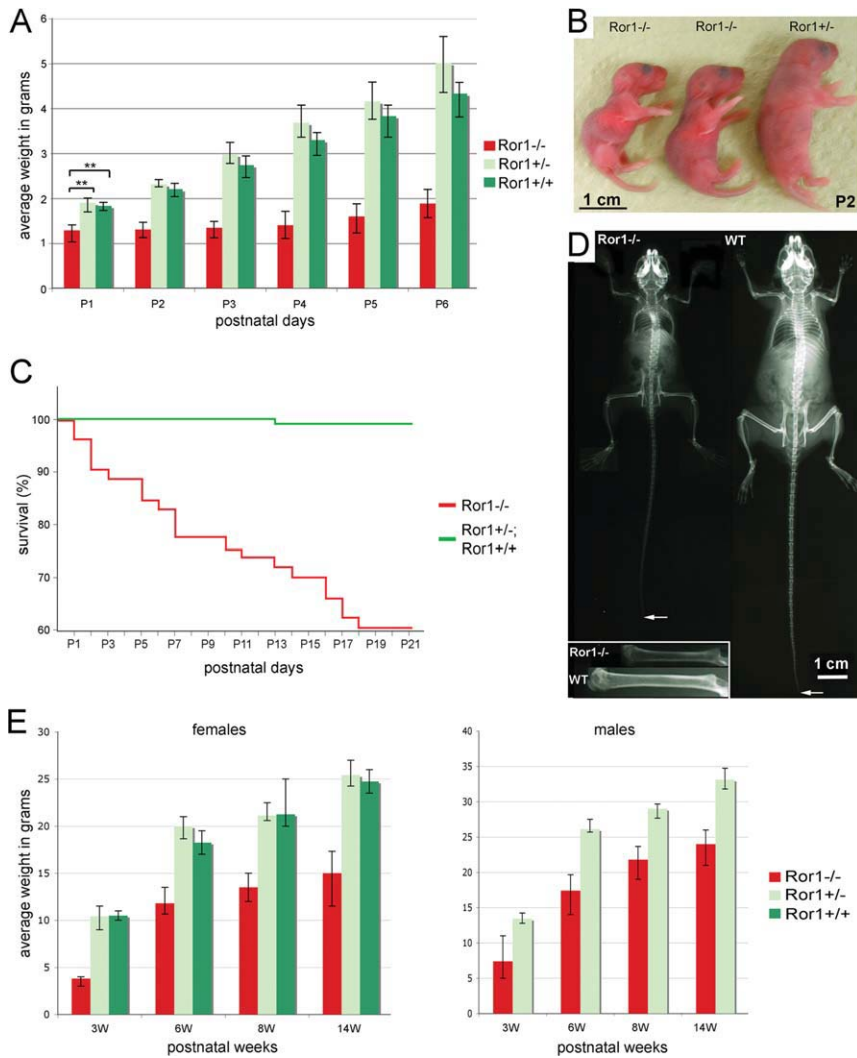
4E and data not shown). Together, this suggests a possible involvement of sex hormones in the expressivity of the mutant phenotype. Mutant males aged for 13–18 months still showed severe weight reduction (32–60%). However, the difference in size was relatively small (5–10%) compared to their littermate controls (Table 3).

### **Abnormal Ossifications Develop in the Spine of Aged Ror1 Mutants**

In alizarin red/alcian blue-stained skeletal preparations of aged mutant mice (15–18 months), we observed abnormal mineralization in the intervertebral discs of the lower thoracic region (n=2/2; T10–T13; arrowheads in Fig. 5A) and occasionally within un-fused sternal synchondroses (data not shown). Abnormal ossification within the axial skeleton could also be observed in microCTs of the lower thoracic spine of 15–18-month-old male mice (n=2/3; arrows in Fig. 5B). In addition, we noticed that there were abnormal ossifications between the spine and the proximal ends of the ribs (white arrowheads in Fig. 5C). The reduction in cortical bone thickness was also visible in the microCTs of the ribs and vertebral bodies (Fig. 5C and data not shown).

### **IGFI Serum Levels Are Reduced in Ror1 Mutants**

Given that the hole in the basisphenoid bone of *Ror1*<sup>-/-</sup> embryos was located directly below the pituitary gland (see Fig. 6A), we suspected that the postnatal growth retardation might be due to altered hormone production by the pituitary gland. Thus, we examined the specification of different hormone-producing cells using immunohisto-chemical staining for growth hormone (GH), thyroid-stimulating hormone beta (TSH $\beta$ ), luteinizing hormone alpha and beta (LH $\alpha$ ,  $\beta$ ), and adrenocorticotropin (ACTH) on E17.5 and P2 sagittal sections. However, no obvious differences in hormone staining were detected between wild-type and *Ror1* mutant pituitaries at both stages of development (Fig. 6A and data not shown). Older pituitary glands of *Ror1*-deficient animals were slightly hypoplastic and



had a different shape compared to wild-type and heterozygous littermate controls (Fig. 6B and data not shown). Western blots on pituitary gland extracts of P17 and P19 old littermates revealed, however, no difference in GH levels (Fig. 6C). Although GH production seemed not to be affected, it's possible that the levels of secreted GH might be altered in *Ror1*<sup>-/-</sup> animals. Since GH synthesis and release from pituitary

**Fig. 4.** Postnatal growth retardation and reduced survival of *Ror1* mutant mice. **A:** Bar graph showing weight reduction of the *Ror1* mutants ( $n = 6-9$ ) at postnatal days P1-P6 compared to their heterozygous ( $n = 8$ ) and wild type ( $n = 8$ ) littermates.  $**P = 0.0001$  (based on two-tailed Student's *t*-test). **B:** Pictures of P2 old pups showing size reduction of mutants compared to heterozygous littermate. **C:** Kaplan Meier survival plot of *Ror1* mutants ( $n = 53$ ; red line) compared to heterozygous and wild type littermates ( $n = 152$ ; green line) until weaning in percent survival. **D:** X-ray picture of 3-month-old *Ror1*<sup>-/-</sup> (left) and *Ror1*<sup>+/+</sup> (right) female littermates showing size reduction (white arrows point at the tip of the tails) and reduced bone density and cortical thickness of the mutant *Ror1*<sup>-/-</sup> femur compared to the control (WT) in the inset ( $n = 3$ ). **E:** Bar graphs showing weight reduction of mutant females (*Ror1*<sup>-/-</sup>  $n = 5$ ; *Ror1*<sup>+/-</sup>  $n = 7$ ; *Ror1*<sup>+/+</sup>  $n = 4$ ) and males (*Ror1*<sup>-/-</sup>  $n = 5$ ; *Ror1*<sup>+/-</sup>  $n = 9$ ) at 3, 6, 8, and 14 weeks of age, compared to littermate controls. Note: The males used in this study were derived from *Ror1*<sup>-/-</sup> and *Ror1*<sup>+/-</sup> intercrosses; hence, no wild-type littermates were available for comparison.

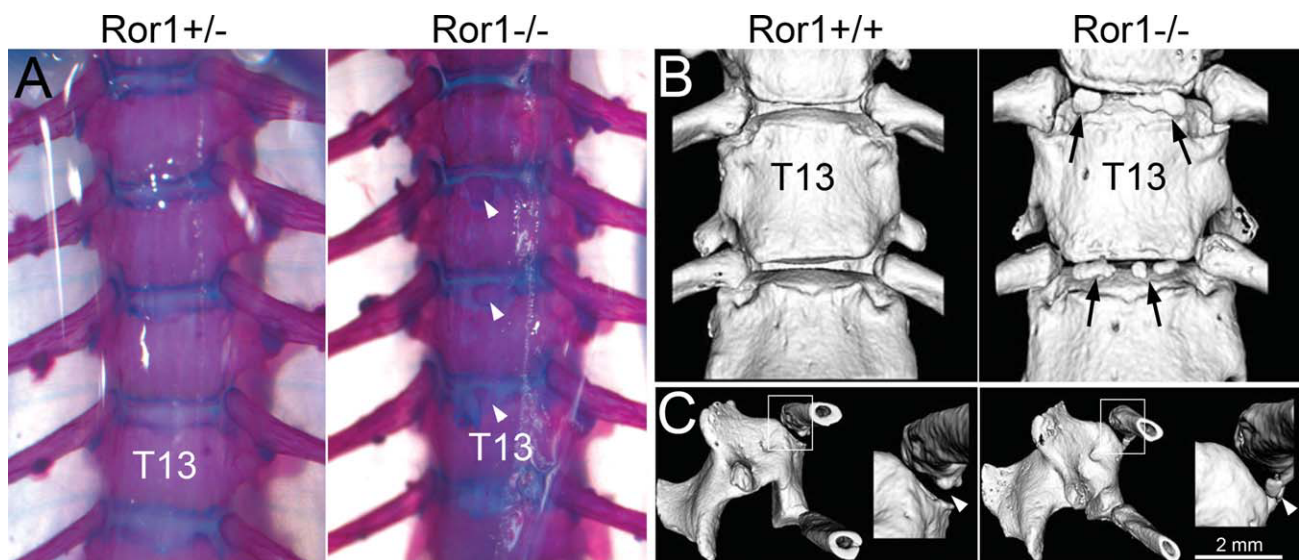


**Fig. 5.** Alterations in the aged skeleton. **A:** Spines of 18-month-old *Ror1*<sup>+/-</sup> and *Ror1*<sup>-/-</sup> males stained with alizarin red/alcian blue, showing abnormal mineralization in the intervertebral discs (white arrowheads) between thoracic segments T10-T13 of the mutant. **B:** MicroCTs of 18-month-old *Ror1*<sup>+/-</sup> and *Ror1*<sup>-/-</sup> males showing abnormal mineralization in the intervertebral discs (black arrows) of the mutant spine. **C:** MicroCTs of the same specimens showing abnormal mineralization in the costovertebral joint of the mutant (white arrowhead).

**TABLE 2. Bone Densitometry Data of Femurs of 3–4-Month-Old Mice<sup>a</sup>**

Genotype	Sex	Age (wk)	Cross-sect area (mm)	Total BMD Trab (mg/cm <sup>3</sup> )	BMD (mg/cm <sup>3</sup> )	Cort. thickness (mm)
<b>Femoral shaft</b>						
Wt (n=3)	F	15	1.92±0.16	699±49	—	0.232±0.008
Het (n=6)	F	15	1.88±0.13	675±31	0.223±0.011	
Mut (n=4)	F	15	1.36±0.11	580±52	—	0.172±0.020
Het (n=2)	M	14	2.54±0.03	660±7	—	0.247±0.005
Mut (n=2)	M	14	1.94±0.08	645±84	—	0.219±0.014
<b>Femoral metaphysis</b>						
Wt (n=3)	F	15	3.38±0.20	499±23	168±11	0.207±0.016
Het (n=6)	F	15	3.41±0.18	490±28	165±12	0.203±0.013
Mut (n=4)	F	15	2.53±0.32	376±38	145±10	0.122±0.028
Het (n=2)	M	14	4.20±0.02	510±47	228±25	0.226±0.032
Mut (n=2)	M	14	3.24±0.40	427±70	172±17	0.155±0.028

<sup>a</sup>BMD, bone mineral density; Cort., cortical; wk, weeks; F, female; M, male; —, not applicable.

**TABLE 3. Comparison of Weight and Size in 13–18-Month- (M) Old *Ror1* Mutants and Littermates**

Genotype	Age (M)	Weight (g)	Size (cm)
Het	18	46	18.2
Mut	18	29	17.5
Wt	16	52	18.7
Het	16	51	19
Mut	16	35	18
Wt	15	41	18.5
Het	15	42	18.5
Mut	15	23	16.5
Het	13	45	17.7
Mut <sup>a</sup>	13	18	16

<sup>a</sup>Cystic right kidney, left seminal vesicle enlarged.

somatotrophs is pulsatile, the serum GH levels fluctuate accordingly. Thus, instead of measuring the serum GH levels we measured the serum levels of IGF-I, since they directly depend on GH levels. The IGF-I levels were indeed reduced in 3-month-old male and female *Ror1* mutant animals (Fig. 6D).

### Urogenital Defects in *Ror1* Mutant Animals

Approximately 90% of the *Ror1* mutant females had an abnormal vagina with an imperforated hymen and could, therefore, not reproduce (Fig. 7A). With age, these *Ror1*<sup>-/-</sup> females accumulated liquid and cellular material in their uteri resulting in a swelling of the uteri and abdomen (Fig. 7B, C). Almost all *Ror1* mutant males tested could reproduce normally, but 3/7 dissected *Ror1*<sup>-/-</sup> males showed

abnormal seminal vesicles that were either cystic or solid and unilaterally enlarged (Fig. 7D, D'). Approximately 30% (5/17) of the *Ror1*<sup>-/-</sup> mice had

abnormal kidneys, where double kidneys and double ureters were present unilaterally (Fig. 7E). All of the mutants with kidney defects had been found dead within the first week, with the exception of one male that was sacrificed at the age of 13 months and had a cystic right kidney (see Table 1). In addition to the urogenital defects, we noticed that the mutant animals had almost no subcutaneous fat and that the visceral fat pads associated with the urogenital system were also reduced in size (Fig. 7D, F).

### DISCUSSION

*Ror1* mutants have previously been reported to die shortly after birth due to defects in lung maturation (Nomi et al., 2001). Currently, we have no explanation for the increased postnatal

**Fig. 6.** Analysis of the pituitary gland. **A:** Sagittal sections through the skull and the pituitary gland of wild-type and *Ror1*<sup>-/-</sup> littermates at P0 stained with von Kossa/alcan blue (AB) and at P2 stained with antibodies to hormones produced by specific subpopulations of the anterior lobe: growth hormone (GH), thyroid-stimulating hormone  $\beta$  subunit (TSH $\beta$ ), luteinizing hormone  $\alpha$  (LH $\alpha$ ) and  $\beta$  (LH $\beta$ ) subunits, and adrenocorticotrophic hormone (ACTH). **B:** Morphological appearance of pituitary gland at P17. **C:** Western blot for growth hormone (GH) and tubulin (tub) from P17 old males and females showing no significant differences in pituitary GH levels between mutants and littermate controls. Note: Brackets indicate corresponding littermates. **D:** Blot of IGF serum levels from 2–3-month-old males and females, showing reduced IGF serum levels in *Ror1*<sup>-/-</sup> males and females (red bars) compared to their littermate controls (n = 1 for each genotype, IGF-serum levels of each specimen were determined by ELISA in duplicates).

**Fig. 7.** Non-skeletal defects in *Ror1* mutant adult animals. **A:** Abnormal vagina in the *Ror1* mutant female (on the right). **B:** Swelling of the uteri in a *Ror1* mutant female (on the right). **C:** Dissected uteri of wild-type and *Ror1* mutant females. **D:** Abnormal seminal vesicles (sv) in *Ror1* mutant male (right side) and reduced urogenital fat pads (fp) attached to the testis (t), bl, bladder. **D':** Fixed genital tract of a *Ror1* mutant male, showing enlargement of one of the seminal vesicles. **E:** Kidneys of wild-type (left) and *Ror1* mutant (right) newborn animals, showing unilateral double kidney in the *Ror1* mutant. Note: The adrenal glands in the *Ror1* mutant were lost during preparation. **F:** P18 old skinned wild-type (top) and *Ror1* mutant (bottom) specimens, showing absence of subcutane white adipose tissue (arrows) in the mutant.

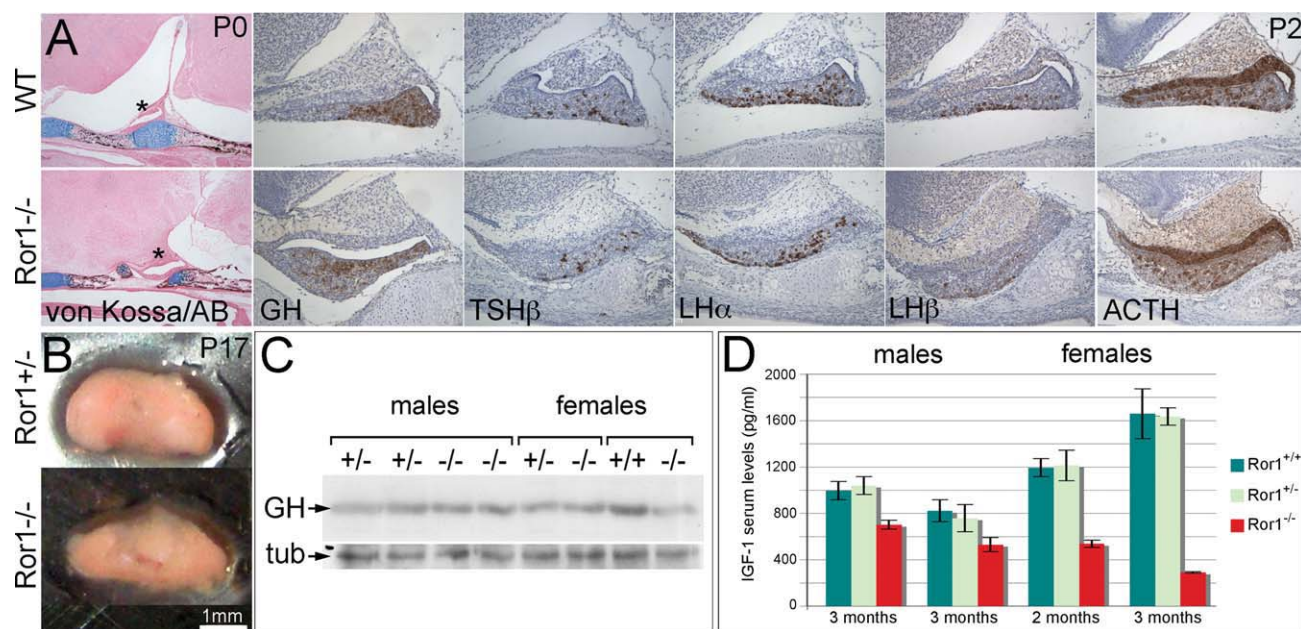


Fig. 6.

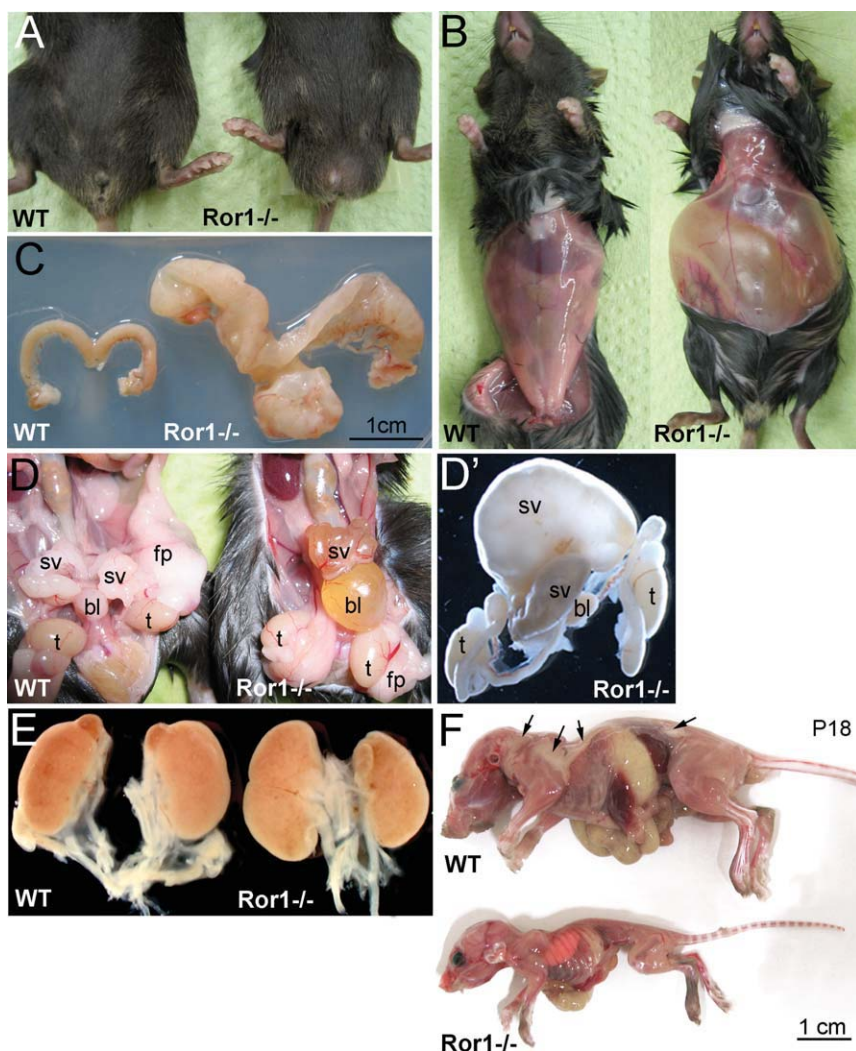


Fig. 7.

survival of *Ror1* mutants that were bred in Vienna, particularly since *Ror1* mice were maintained in a C57Bl/6 background. Nevertheless, we cannot rule out subtle differences between the C57Bl/6 strains in the two geographically distinct locations. The fact that we still observed a high lethality rate for the *Ror1* mutants within the first few days suggests a fitness weakness of *Ror1* mutants. In contrast to *Ror2*, loss-of *Ror1* activity resulted only in minor skeletal defects, affecting primarily the sternum, the basisphenoid bone, and the axial element C2 during embryonic development. *Ror1* and *Ror2* have been implicated as co-receptors in Wnt-signaling and for *Ror2* it was shown that it can modulate Gdf5/BMP receptor signaling (Sammar et al., 2004; Green et al., 2008). As such, it is interesting to note that a similar phenotype in the basisphenoid bone has been observed in embryos double mutant for *Tcf4/Lef1* during development at E15.5 and in mutants for *Bmp7* or conditional mutants of the Tgf-beta receptor 2, *Tgfb2*<sup>ΔCol2</sup> (Jena et al., 1997; Baffi et al., 2004; Brugmann et al., 2007). Furthermore, it is interesting to note that double mutants for the heparan sulfate 6-O-endosulfatase genes *Sulf1* and *Sulf2*, which alter sulfate modification of heparan molecules in the extracellular matrix, showed a similar

phenotype in the basisphenoid bone (Holst et al., 2007; Ratzka et al., 2008). In these mutants, signaling of several growth factors (including Wnts, hedgehogs, and fibroblast growth factors) is probably affected. Mutants for *Gli3*<sup>Δ699/Δ699</sup>, which encodes only a N-terminal truncated version of Gli3 solely acting as a repressor, also have a hole in the basisphenoid bone (Bose et al., 2002). Fusions of sternbrae or ectopic mineralization within the fibrocartilage separating the sternbrae have been reported also in *Sulf1/2* double mutants and in mutants for the TGFβ/BMP family members, *Bmp5* and *Gdf5* (Storm and Kingsley, 1996; Holst et al., 2007; Ratzka et al., 2008). Thus, given the phenotypic similarities, it might be possible that in analogy to *Ror2*, *Ror1* might not only interact with Wnt-ligands altering Wnt-signaling, but might also modulate TGFβ/BMP signaling.

Besides the patterning defects in certain skeletal elements, we noticed postnatal alterations in the growth plates of the long bones of *Ror1* mutants. Here the zones of prehypertrophic and hypertrophic chondrocytes were reduced from postnatal day 2 onwards. Based on our analyses, it seemed that primarily the zone of immature hypertrophic chondrocytes, in which the cells do not have a mineralized matrix, nor do they express *Opn*, is severely reduced or maybe even lost. This specific defect in chondrocyte maturation might contribute to the fact that the appearance of the secondary ossification centers was delayed as well. Currently, we have no explanation for the molecular nature of the specific defect. The previous study by Nomi and colleagues suggests that *Ror1* has redundant functions with *Ror2* during embryonic skeletal development (Nomi et al., 2001). However, the study gave no insights into the underlying mechanism explaining the further shortening of the skeletal elements particularly in the stylopode region. *Ror2* seems to be regulating chondrocyte maturation primarily at the level of prehypertrophic chondrocytes (Schwabe et al., 2004). Our analysis suggests that in contrast to *Ror2*, *Ror1* might be required at a slightly different step of chondrocyte maturation acting primarily in immature hypertrophic chondrocytes. This

could explain the additional decrease in overall length and of the mineralized zone of the stylopode elements, humerus and femur, upon loss of *Ror1* in a *Ror2* mutant background. This would also explain why there was no significant effect on zeugopode elements such as the ulna and radius upon additional removal of *Ror1* (Nomi et al., 2001). Here the differentiation of prehypertrophic and hypertrophic chondrocytes is already severely delayed in *Ror2* single mutants, while it still occurs in the stylopode at E15.5 (Schwabe et al., 2004).

In addition to the specific reduction in immature hypertrophic chondrocytes, the postnatal growth deficiency might in part be influenced by the reduction in IGF-I serum levels but it is probably also influenced by sex hormones given that the differences in size are much more pronounced in females than in males. Whether the reduced IGF-I serum levels are related to altered growth hormone production due to the morphological alteration in the basisphenoid bone and the associated pituitary gland deformation or if they might be due to local *Ror1* activity in IGF-I-producing organs is currently unclear. While *Ror1* is expressed fairly broadly in the organism, it is not expressed in the liver, which is the major site of IGF-I production (Al-Shawi et al., 2001; Baskar et al., 2008). Concomitantly, liver-specific deletion of *Igf-1* does not affect growth of the appendicular skeleton (Yakar et al., 1999; Sjogren et al., 2002). Thus, local IGF-I production in the growth plate of the long bones is probably affected in *Ror1* mutants, given the reduction in the hypertrophic zone that is the predominant region in which *Igf-1* is transcribed postnatally (Reinecke et al., 2000; Smink et al., 2002). IGF-I has been shown to stimulate hypertrophic chondrocyte differentiation (Mushtaq et al., 2004). Thus, a reduction in IGF-I-producing hypertrophic chondrocytes might exaggerate the phenotype. Our phenotypic analysis suggests that *Ror1* activity is required for postnatal growth and hypertrophic chondrocyte differentiation and that the phenotype is possibly mediated in part via the GH/IGF-I system. Since *Ror1* is fairly broadly expressed and not highly expressed in the chondro-

cytes, it is currently unclear to what extent the growth plate phenotype is due to a *Ror1* activity requirement particularly in chondrocytes. In addition, it is well known that cortical bone mass and size is severely reduced in *IGF-I*-ablated mice (Moerth et al., 2007). Therefore, it remains to be determined whether the cortical bone osteopenia observed in *Ror1* mutants is caused by lack of *Ror1* and concomitantly reduced Wnt signaling in periosteal osteoblasts, or by an indirect effect through the GH/IGF-1 axis.

Furthermore, our phenotypic analysis revealed a requirement for *Ror1* in the urogenital system. The relatively low penetrance of the kidney defects makes it difficult to study the underlying mechanisms. In addition to *Ror1*, *Ror2* is also expressed in the urogenital tract (Al-Shawi et al., 2001). Interestingly, we noticed in *Ror2* mutants a very similar kidney phenotype with double ureters, unilateral or bilateral double kidneys, cystic kidneys, or even sporadic agenesis of one kidney in 30–40% of *Ror2* mutants (C. Hartmann, unpublished observation). Thus, it is possible that *Ror1* and *Ror2* act redundantly in kidney development, although no defect in kidney development has been reported in the previous double mutant analysis (Nomi et al., 2001). *Ror1* and *Ror2* could possibly modulate Wnt or TGFβ/BMP-signaling during kidney development, as Wnt-signaling as well as TGFβ/BMP-signaling have been functionally implicated in different aspects of kidney development (Martinez and Bertram, 2003; Pulkkinen et al., 2008).

## EXPERIMENTAL PROCEDURES

### Mouse Husbandry

The generation of the *Ror1* mutant allele has been previously described (Nomi et al., 2001). The *Ror1* strain was maintained in a C57Bl/6 background. Mutants were generated by intercrosses of heterozygous mice, or through breeding of homozygous males with heterozygous females to increase the number of mutant offspring. Genotyping of mice was performed by PCR using the following primer pairs: for detection of the 1.1-kb wild-type allele the WT\_for-primer

5' GGCAACAAATGGCAAGAAAGTGTGTC and WT\_rev-primer 5' GAAA TGGAAATCCTTAGACTCCGTTATC were used. For detection of the 1.1-kb mutant allele, the WT\_for-primer was used in combination with the neo-primer 5' ATCGCCTTCTATCGCCTTCTTGACGAG.

### Skeletal Preparations, MicroCT, and Bone Densitometry

For the alcian blue/alizarin red staining of newborns, postnatal, and adult mouse skeletons, the mice were sacrificed, skinned, eviscerated, fixed in 95% ethanol, and stained according to McLeod (1980). Harvested organs were visually inspected for abnormalities. Three-dimensional medium-resolution images were obtained from the skulls, spine, ribs, and digits of *Ror1*<sup>-/-</sup> and control mice (*Ror1*<sup>+/-</sup>; *Ror1*<sup>+/+</sup>) using microcomputed tomography (eXplore locus SP, GE Healthcare, London, Ontario, Canada). Scans were taken at 28- $\mu$ m isotropic resolution and 720 projections were acquired over an angular range of 360°. Images were reconstructed and thresholded to distinguish bone voxels with MicroView software version 5.2.2 (GE Healthcare, Buckinghamshire, UK). One threshold was chosen for all specimens or as previously described (Amarilio et al., 2007). Volumetric bone mineral density (BMD) of the femurs was measured by peripheral quantitative computed tomography (pQCT) using a XCT Research M+ pQCT machine (Stratec Medizintechnik, Pforzheim, Germany) as described (Schneider et al., 2009). One slice (0.2 mm thick) in the mid-diaphysis of the femur and 3 slices in the distal femoral metaphysis located 1.5, 2, and 2.5 mm proximal to the articular surface of the knee joint were measured. BMD values of the distal femoral metaphysis were calculated as the mean over 3 slices. A voxel size of 0.070 mm and a threshold of 600 mg/cm<sup>3</sup> were used for calculation of BMD.

### Histology and In Situ Hybridizations

For histology and section in situ hybridizations, material from embryos

and pups was dissected, washed in PBS, and fixed overnight in 4% PFA/PBS, dehydrated to 70% ethanol, and processed using a standard program of the Tissue-Tek VIP5 Vacuum Infiltration Processor (Sakura, Torrance, CA). Processed tissue was embedded in paraffin and sectioned at 5  $\mu$ m. Hematoxylin/eosin staining was performed using standard protocols. Alcian blue/van Kossa staining on sections was performed as follows: tissue was rehydrated, washed twice in deionized water, exposed for 60 min in 2% silver-nitrate solution to a 60-W lamp, washed three times in deionized water, incubated for 2 min in 1% acetic acid, stained with alcian blue solution (pH 2.2) for 15 min, washed in 1% acetic acid, dehydrated into 75% ethanol, counterstained for 30 sec with eosin, destained with 100% ethanol and xylene, and mounted using DPX (Fluka, St. Louis, MO). Whole mount and section in situ hybridizations were done as previously described (Murtaugh et al., 1999; Riddle et al., 1993).

### Immunohistochemistry, Western Blot, and Elisa for IGF1 Serum Levels

Immunohistochemistry for the following hormone precursors, GH (1:10,000), TSH $\beta$  (1:2,000), LH $\alpha$  (1:2,000), LH $\beta$  (1:2,000), and ACTH (1:3,000) was performed on paraffin sections of the pituitaries from E17 embryos and P2 mice. Antibodies were obtained from the National Hormone and Pituitary Program and immunohistochemistry was performed using the Ventana. Briefly, sections were dewaxed and rehydrated; antigen-retrieval was done using citrate buffer pH 6.0. Western blots to determine GH protein levels were performed on 50- $\mu$ g protein extracts from dissected pituitaries from P17 & P19 mice ( $\alpha$ -GH at a dilution of 1:2,000). IGF1 serum levels were determined in duplicates from the plasma of *Ror1*<sup>-/-</sup> and control mice at 2 and 3 months of age using an IGF-I Elisa assay following the manufacturer's instructions (Quantikine Kit, R&D Systems, Minneapolis, MN).

### ACKNOWLEDGMENTS

We thank Christiane Schöler, Martin Glösmann, and Claudia Bergow for

help with the pQCT analysis, and Vukoslav Kommenovic for technical assistance. The IMP is supported by Boehringer Ingelheim. N.L. was supported by the Austrian Science Found (FWF grant P19281-B16).

### REFERENCES

- Afzal AR, Rajab A, Fenske CD, Oldridge M, Elanko N, Ternes-Pereira E, Tuysuz B, Murday VA, Patton MA, Wilkie AO, Jeffery S. 2000. Recessive Robinow syndrome, allelic to dominant brachydactyly type B, is caused by mutation of ROR2. *Nat Genet* 25:419–422.
- Al-Shawi R, Ashton SV, Underwood C, Simons JP. 2001. Expression of the *Ror1* and *Ror2* receptor tyrosine kinase genes during mouse development. *Dev Genes Evol* 211:161–171.
- Amarilio R, Viukov SV, Sharir A, Eshkar-Oren I, Johnson RS, Zelzer E. 2007. HIF1 $\alpha$  regulation of Sox9 is necessary to maintain differentiation of hypoxic prechondrogenic cells during early skeletogenesis. *Development* 134:3917–3928.
- Baffi MO, Slattery E, Sohn P, Moses HL, Chytil A, Serra R. 2004. Conditional deletion of the TGF-beta type II receptor in Col2a expressing cells results in defects in the axial skeleton without alterations in chondrocyte differentiation or embryonic development of long bones. *Dev Biol* 276:124–142.
- Baskar S, Kwong KY, Hofer T, Levy JM, Kennedy MG, Lee E, Staudt LM, Wilson WH, Wiestner A, Rader C. 2008. Unique cell surface expression of receptor tyrosine kinase ROR1 in human B-cell chronic lymphocytic leukemia. *Clin Cancer Res* 14:396–404.
- Bose J, Grotewold L, Ruther U. 2002. Pallister-Hall syndrome phenotype in mice mutant for Gli3. *Hum Mol Genet* 11:1129–1135.
- Brugmann SA, Goodnough LH, Gregorieff A, Leucht P, ten Berge D, Fuerer C, Clevers H, Nusse R, Helms JA. 2007. Wnt signaling mediates regional specification in the vertebrate face. *Development* 134:3283–3295.
- Daneshmanesh AH, Mikaelsson E, Jeddih-Tehrani M, Bayat AA, Ghods R, Ostadkarampour M, Akhondi M, Lagercrantz S, Larsson C, Osterborg A, Shokri F, Mellstedt H, Rabbani H. 2008. *Ror1*, a cell surface receptor tyrosine kinase is expressed in chronic lymphocytic leukemia and may serve as a putative target for therapy. *Int J Cancer* 123:1190–1195.
- DeChiara TM, Kimble RB, Poueymirou WT, Rojas J, Masiakowski P, Valenzuela DM, Yancopoulos GD. 2000. *Ror2*, encoding a receptor-like tyrosine kinase, is required for cartilage and growth plate development. *Nat Genet* 24:271–274.
- Enomoto M, Hayakawa S, Itsukushima S, Ren DY, Matsuo M, Tamada K,

- Oneyama C, Okada M, Takumi T, Nishita M, Minami Y. 2009. Autonomous regulation of osteosarcoma cell invasiveness by Wnt5a/Ror2 signaling. *Oncogene* 28:3197–3208.
- Fukuda T, Chen L, Endo T, Tang L, Lu D, Castro JE, Widhopf GF, 2nd, Rassenti LZ, Cantwell MJ, Prussak CE, Carson DA, Kipps TJ. 2008. Antisera induced by infusions of autologous Ad-CD154-leukemia B cells identify ROR1 as an oncofetal antigen and receptor for Wnt5a. *Proc Natl Acad Sci USA* 105:3047–3052.
- Green JL, Kuntz SG, Sternberg PW. 2008. Ror receptor tyrosine kinases: orphans no more. *Trends Cell Biol* 18:536–544.
- Hamamy H, Saleh N, Oldridge M, Al-Hadidy A, Ajlouni K. 2006. Brachydactyly type B1: report of a family with de novo ROR2 mutation. *Clin Genet* 70:538–540.
- He F, Xiong W, Yu X, Espinoza-Lewis R, Liu C, Gu S, Nishita M, Suzuki K, Yamada G, Minami Y, Chen Y. 2008. Wnt5a regulates directional cell migration and cell proliferation via Ror2-mediated noncanonical pathway in mammalian palate development. *Development* 135:3871–3879.
- Hikasa H, Shibata M, Hiratani I, Taira M. 2002. The Xenopus receptor tyrosine kinase Xror2 modulates morphogenetic movements of the axial mesoderm and neuroectoderm via Wnt signaling. *Development* 129:5227–5239.
- Holst CR, Bou-Reslan H, Gore BB, Wong K, Grant D, Chalasani S, Carano RA, Frantz GD, Tessier-Lavigne M, Bolon B, French DM, Ashkenazi A. 2007. Secreted sulfatases Sulf1 and Sulf2 have overlapping yet essential roles in mouse neonatal survival. *PLoS One* 2:e575.
- Jena N, Martin-Seisdedos C, McCue P, Croce CM. 1997. BMP7 null mutation in mice: developmental defects in skeleton, kidney, and eye. *Exp Cell Res* 230:28–37.
- Kobayashi M, Shibuya Y, Takeuchi J, Murata M, Suzuki H, Yokoo S, Umeda M, Minami Y, Komori T. 2009. Ror2 expression in squamous cell carcinoma and epithelial dysplasia of the oral cavity. *Oral Surg Oral Med Oral Pathol Oral Radiol Endod* 107:398–406.
- Li C, Chen H, Hu L, Xing Y, Sasaki T, Villosis MF, Li J, Nishita M, Minami Y, Minoo P. 2008. Ror2 modulates the canonical Wnt signaling in lung epithelial cells through cooperation with Fzd2. *BMC Mol Biol* 9:11.
- Liu Y, Rubin B, Bodine PV, Billiard J. 2008. Wnt5a induces homodimerization and activation of Ror2 receptor tyrosine kinase. *J Cell Biochem* 105:497–502.
- MacKeigan JP, Murphy LO, Blenis J. 2005. Sensitized RNAi screen of human kinases and phosphatases identifies new regulators of apoptosis and chemoresistance. *Nat Cell Biol* 7:591–600.
- Martinez G, Bertram JF. 2003. Organisation of bone morphogenetic proteins in renal development. *Nephron Exp Nephrol* 93:e18–22.
- Matsuda T, Nomi M, Ikeya M, Kani S, Oishi I, Terashima T, Takada S, Minami Y. 2001. Expression of the receptor tyrosine kinase genes, Ror1 and Ror2, during mouse development. *Mech Dev* 105:153–156.
- McLeod MJ. 1980. Differential staining of cartilage and bone in whole mouse fetuses by alcian blue and alizarin red S. *Teratology* 22:299–301.
- Mikels AJ, Nusse R. 2006. Purified Wnt5a protein activates or inhibits beta-catenin-TCF signaling depending on receptor context. *PLoS Biol* 4:e115.
- Minami Y, Oishi I, Endo M, Nishita M. 2009. Ror-family receptor tyrosine kinases in noncanonical Wnt signaling: Their implications in developmental morphogenesis and human diseases. *Dev Dyn* 239:1–15.
- Moerth C, Schneider MR, Renner-Mueller I, Blutke A, Elmlinger MW, Erben RG, Camacho-Hubner C, Hoefflich A, Wolf E. 2007. Postnatally elevated levels of insulin-like growth factor (IGF)-II fail to rescue the dwarfism of IGF-I-deficient mice except kidney weight. *Endocrinology* 148:441–451.
- Morioka K, Tanikawa C, Ochi K, Daigo Y, Katagiri T, Kawano H, Kawaguchi H, Myoui A, Yoshikawa H, Naka N, Araki N, Kudawara I, Ieguchi M, Nakamura K, Nakamura Y, Matsuda K. 2009. Orphan receptor tyrosine kinase ROR2 as a potential therapeutic target for osteosarcoma. *Cancer Sci* 100:1227–1233.
- Murtaugh LC, Chyung JH, Lassar AB. 1999. Sonic hedgehog promotes somitic chondrogenesis by altering the cellular response to BMP signaling. *Genes Dev* 13:225–237.
- Mushtaq T, Bijman P, Ahmed SF, Farquharson C. 2004. Insulin-like growth factor-I augments chondrocyte hypertrophy and reverses glucocorticoid-mediated growth retardation in fetal mice metatarsal cultures. *Endocrinology* 145:2478–2486.
- Nomi M, Oishi I, Kani S, Suzuki H, Matsuda T, Yoda A, Kitamura M, Itoh K, Takeuchi S, Takeda K, Akira S, Ikeya M, Takada S, Minami Y. 2001. Loss of mRor1 enhances the heart and skeletal abnormalities in mRor2-deficient mice: redundant and pleiotropic functions of mRor1 and mRor2 receptor tyrosine kinases. *Mol Cell Biol* 21:8329–8335.
- O'Connell MP, Fiori JL, Xu M, Carter AD, Frank BP, Camilli TC, French AD, Dissanayake SK, Indig FE, Bernier M, Taub DD, Hewitt SM, Weeraratna AT. 2010. The orphan tyrosine kinase receptor, ROR2, mediates Wnt5A signaling in metastatic melanoma. *Oncogene* 29:34–44.
- Oishi I, Takeuchi S, Hashimoto R, Nagabukuro A, Ueda T, Liu ZJ, Hatta T, Akira S, Matsuda Y, Yamamura H, Otani H, Minami Y. 1999. Spatio-temporally regulated expression of receptor tyrosine kinases, mRor1, mRor2, during mouse development: implications in development and function of the nervous system. *Genes Cells* 4:41–56.
- Oishi I, Suzuki H, Oishi N, Takada R, Kani S, Ohkawara B, Koshida I, Suzuki K, Yamada G, Schwabe GC, Mundlos S, Shibuya H, Takada S, Minami Y. 2003. The receptor tyrosine kinase Ror2 is involved in non-canonical Wnt5a/JNK signalling pathway. *Genes Cells* 8:645–654.
- Oldridge M, Fortuna AM, Maringa M, Proping P, Mansour S, Pollitt C, DeChiara TM, Kimble RB, Valenzuela DM, Yancopoulos GD, Wilkie AO. 2000. Dominant mutations in ROR2, encoding an orphan receptor tyrosine kinase, cause brachydactyly type B. *Nat Genet* 24:275–278.
- Paganoni S, Ferreira A. 2003. Expression and subcellular localization of Ror tyrosine kinase receptors are developmentally regulated in cultured hippocampal neurons. *J Neurosci Res* 73:429–440.
- Pulkkinen K, Murugan S, Vainio S. 2008. Wnt signaling in kidney development and disease. *Organogenesis* 4:55–59.
- Ratzka A, Kalus I, Moser M, Dierks T, Mundlos S, Vortkamp A. 2008. Redundant function of the heparan sulfate 6-O-endosulfatases Sulf1 and Sulf2 during skeletal development. *Dev Dyn* 237:339–353.
- Raz R, Stricker S, Gazzo E, Clor JL, Witte F, Nistala H, Zabski S, Pereira RC, Stadmeier L, Wang X, Gowen L, Sleeman MW, Yancopoulos GD, Canalis E, Mundlos S, Valenzuela DM, Economides AN. 2008. The mutation ROR2W749X, linked to human BDB, is a recessive mutation in the mouse, causing brachydactyly, mediating patterning of joints and modeling recessive Robinow syndrome. *Development* 135:1713–1723.
- Reinecke M, Schmid AC, Heyberger-Meyer B, Hunziker EB, Zapf J. 2000. Effect of growth hormone and insulin-like growth factor I (IGF-I) on the expression of IGF-I messenger ribonucleic acid and peptide in rat tibial growth plate and articular chondrocytes in vivo. *Endocrinology* 141:2847–2853.
- Riddle RD, Johnson RL, Laufer E, Tabin C. 1993. Sonic hedgehog mediates the polarizing activity of the ZPA. *Cell* 75:1401–1416.
- Rodriguez-Niedenfuhr M, Prols F, Christ B. 2004. Expression and regulation of ROR-1 during early avian limb development. *Anat Embryol (Berl)* 207:495–502.
- Saldanha J, Singh J, Mahadevan D. 1998. Identification of a Frizzled-like cysteine rich domain in the extracellular region of developmental receptor tyrosine kinases. *Protein Sci* 7:1632–1635.
- Sammar M, Stricker S, Schwabe GC, Sieber C, Hartung A, Hanke M, Oishi I, Pohl J, Minami Y, Sebald W, Mundlos S, Knaus P. 2004. Modulation of GDF5/BRI-b signalling through interaction with the tyrosine kinase receptor Ror2. *Genes Cells* 9:1227–1238.
- Schneider MR, Mayer-Roenne B, Dahlhoff M, Proell V, Weber K, Wolf E, Erben RG. 2009. High cortical bone mass phenotype in betacellulin transgenic mice is EGFR dependent. *J Bone Miner Res* 24:455–467.

- Schwabe GC, Tinschert S, Buschow C, Meinecke P, Wolff G, Gillessen-Kaesbach G, Oldridge M, Wilkie AO, Komec R, Mundlos S. 2000. Distinct mutations in the receptor tyrosine kinase gene ROR2 cause brachydactyly type B. *Am J Hum Genet* 67:822–831.
- Schwabe GC, Trepzick B, Suring K, Brieske N, Tucker AS, Sharpe PT, Minami Y, Mundlos S. 2004. Ror2 knockout mouse as a model for the developmental pathology of autosomal recessive Robinow syndrome. *Dev Dyn* 229:400–410.
- Shabani M, Asgarian-Omran H, Jeddi-Tehrani M, Vossough P, Faranoush M, Sharifian RA, Toughe GR, Kordmahin M, Khoshnoodi J, Roohi A, Tavooosi N, Mellstedt H, Rabbani H, Shokri F. 2007. Overexpression of orphan receptor tyrosine kinase Ror1 as a putative tumor-associated antigen in Iranian patients with acute lymphoblastic leukemia. *Tumour Biol* 28:318–326.
- Shabani M, Asgarian-Omran H, Vossough P, Sharifian RA, Faranoush M, Ghragozlou S, Khoshnoodi J, Roohi A, Jeddi-Tehrani M, Mellstedt H, Rabbani H, Shokri F. 2008. Expression profile of orphan receptor tyrosine kinase (ROR1) and Wilms' tumor gene 1 (WT1) in different subsets of B-cell acute lymphoblastic leukemia. *Leuk Lymphoma* 49:1360–1367.
- Sjogren K, Jansson JO, Isaksson OG, Ohlsson C. 2002. A model for tissue-specific inducible insulin-like growth factor-I (IGF-I) inactivation to determine the physiological role of liver-derived IGF-I. *Endocrine* 19:249–256.
- Smink JJ, Koster JG, Gresnigt MG, Rooman R, Koedam JA, Van Buul-Offers SC. 2002. IGF and IGF-binding protein expression in the growth plate of normal, dexamethasone-treated and human IGF-II transgenic mice. *J Endocrinol* 175:143–153.
- Storm EE, Kingsley DM. 1996. Joint patterning defects caused by single and double mutations in members of the bone morphogenetic protein (BMP) family. *Development* 122:3969–3979.
- Takeuchi S, Takeda K, Oishi I, Nomi M, Ikeya M, Itoh K, Tamura S, Ueda T, Hatta T, Otani H, Terashima T, Takada S, Yamamura H, Akira S, Minami Y. 2000. Mouse Ror2 receptor tyrosine kinase is required for the heart development and limb formation. *Genes Cells* 5:71–78.
- van Bokhoven H, Celli J, Kayserili H, van Beusekom E, Balci S, Brussel W, Skovby F, Kerr B, Percin EF, Akarsu N, Brunner HG. 2000. Mutation of the gene encoding the ROR2 tyrosine kinase causes autosomal recessive Robinow syndrome. *Nat Genet* 25:423–426.
- Wright TM, Brannon AR, Gordan JD, Mikels AJ, Mitchell C, Chen S, Espinosa I, van de Rijn M, Pruthi R, Wallen E, Edwards L, Nusse R, Rathmell WK. 2009. Ror2, a developmentally regulated kinase, promotes tumor growth potential in renal cell carcinoma. *Oncogene* 28:2513–2523.
- Yakar S, Liu JL, Stannard B, Butler A, Accili D, Sauer B, LeRoith D. 1999. Normal growth and development in the absence of hepatic insulin-like growth factor I. *Proc Natl Acad Sci USA* 96:7324–7329.
- Yoda A, Oishi I, Minami Y. 2003. Expression and function of the Ror-family receptor tyrosine kinases during development: lessons from genetic analyses of nematodes, mice, and humans. *J Recept Signal Transduct Res* 23:1–15.